Richa Dubey, Shruti H. Kulkarni, Sarath Chandra Dantu, Rajlaxmi Panigrahi, Devika M. Sardesai, Nikita Malik, Jhankar D. Acharya, Jeetender Chugh, Shilpy Sharma* and Ashutosh Kumar*

Myricetin protects pancreatic β-cells from human islet amyloid polypeptide (hIAPP) induced cytotoxicity and restores islet function

https://doi.org/10.1515/hsz-2020-0176
Received May 2, 2020; accepted August 25, 2020; published online September 16, 2020

Abstract: The aberrant misfolding and self-assembly of human islet amyloid polypeptide (hIAPP)–a hormone that is co-secreted with insulin from pancreatic β-cells–into toxic oligomers, protofibrils and fibrils has been observed in type 2 diabetes mellitus (T2DM). The formation of these insoluble aggregates has been linked with the death and dysfunction of β-cells. Therefore, hIAPP aggregation has been identified as a therapeutic target for T2DM management. Several natural products are now being investigated for their potential to inhibit hIAPP aggregation and/or disaggregate preformed aggregates. In this study, we attempt to identify the anti-amyloidogenic potential of Myricetin (MYR)- a polyphenolic flavanoid, commonly found in fruits (like *Syzygium cumini*). Our results from biophysical studies indicated that MYR supplementation inhibits hIAPP aggregation and disaggregates preformed fibrils into non-toxic species. This protection was accompanied by inhibition of oxidative stress, reduction in lipid peroxidation and the associated membrane damage and restoration of mitochondrial membrane potential in INS-1E cells. MYR supplementation also reversed the loss of functionality in hIAPP exposed pancreatic islets via restoration of glucose-stimulated insulin secretion. Molecular dynamics simulation studies suggested that MYR molecules interact with the hIAPP pentameric fibril model at the amyloidogenic core region and thus prevents aggregation and distort the fibrils.

Keywords: amyloid; hIAPP; INS-1E; myricetin; pancreatic β-cells; type 2 diabetes mellitus.

***Corresponding authors: Shilpy Sharma, PhD** and **Ashutosh Kumar**, Department of Biotechnology, Savitribai Phule Pune University (Formerly University of Pune), Ganeshkhind, 411007 Pune, Maharashtra, India, E-mail: shilpy.sharma@gmail.com; and Department of Biosciences and Bioengineering, Indian Institute of Technology Bombay, Powai, 400076 Mumbai, Maharashtra, India, E-mail: ashutoshk@iitb.ac.in. https://orcid.org/0000-0001-5900-3140

Richa Dubey, Rajlaxmi Panigrahi and Nikita Malik, Department of Biosciences and Bioengineering, Indian Institute of Technology Bombay, Powai, 400076 Mumbai, Maharashtra, India

Shruti H. Kulkarni and Devika M. Sardesai, Department of Biotechnology, Savitribai Phule Pune University (Formerly University of Pune), Ganeshkhind, 411007 Pune, Maharashtra, India

Sarath Chandra Dantu, Department of Biosciences and Bioengineering, Indian Institute of Technology Bombay, Powai, 400076 Mumbai, Maharashtra, India; Department of Computer Science, Brunel University London, UB83PH Uxbridge, UK

Jhankar D. Acharya, Department of Zoology, Savitribai Phule Pune University (Formerly University of Pune), Ganeshkhind, 411007 Pune, Maharashtra, India

Jeetender Chugh, Department of Chemistry, Indian Institute of Science Education and Research, Homi Bhabha Road, Pashan, 411008 Pune, India; Department of Biology, Indian Institute of Science Education and Research, Homi Bhabha Road, Pashan, 411008 Pune, India

Introduction

The misfolding and aggregation of proteins/peptides leading to the formation of amyloidogenic aggregates has been linked with several human diseases, including Alzheimer's disease, Parkinson's disease, Huntington's disease and Type 2 Diabetes Mellitus (T2DM), etc. (Dobson 2003). The human islet amyloid polypeptide (hIAPP) or amylin is a 37-residue long polypeptide, that is produced and co-secreted along with insulin from the pancreatic β-cells (Marzban et al. 2003; Stridsberg and Wilander 1991). Under normal conditions, hIAPP functions as a satiety hormone and plays an important role in counter-regulating insulin secretion by suppressing food intake and increasing blood glucose levels (Cooper et al. 1988). However, under chronic hyperglycaemic and dyslipidemic conditions associated with T2DM, the amount of hIAPP mRNA expression and protein release increases from the pancreatic islets, thereby resulting in the aggregation of hIAPP into toxic amyloid deposits (Cadavez et al. 2014; Kusakabe et al. 2012; Okada et al. 2016; Pilkington et al. 2016). The formation of these amyloidogenic aggregates has been linked to the β-cells dysfunction

and apoptosis; wherein these aggregates have been detected in >90% of diabetic subjects (Jurgens et al. 2011; Mukherjee et al. 2015).

The aggregation of hIAPP is considered as a non-covalent assembly process that follows a nucleation-elongation mechanism; wherein monomeric proteins aggregate to form small oligomers which further grow to form proto-fibrils and fibrils (Buchanan et al. 2013; Frieden 2007). These hIAPP intermediates interact differently with cell membranes, thereby causing structural perturbations; inducing inflammation, endoplasmic reticulum stress and mitochondrial damage in cells; and hence lead to pancreatic β-cells cell death (Cao et al. 2013). The insulin content and glucose stimulated insulin secretion (GSIS) from pancreatic β-cells is also affected in the presence of these intermediates (Dubey et al. 2017). Therefore, inhibition of hIAPP aggregation and the disaggregation of the pre-formed fibrils are being considered as an attractive strategy for the effective management of T2DM.

Recent studies have reported natural small molecule like terpenoids, flavanoids, etc.; chemically synthesized compounds and peptides; and molecular chaperones and metallic ions; have the potential to inhibit hIAPP aggregation and/or disaggregate the pre-formed hIAPP fibrils (Cadavez et al. 2014; He et al. 2013; Jayakanthan et al. 2009; Li et al. 2014; Ma et al. 2014; Sim et al. 2010). A family of pharmaco-chaperones were studied as modulators that showed multiple target capacity in the aggregation-oligomerization process (Fernández et al. 2018). These pharmaco-chaperons were shown to inhibit and/or delay the aggregation-oligomerization pathway by binding and stabilizing the amyloid-like steric zipper of amyloid structures of hIAPP. Polyphenolic compounds including (−)-epigallocatechin 3-gallate (EGCG), curcumin, resveratrol, and kaempferol have been identified as effective inhibitors against hIAPP aggregation and several other amyloidogenic proteins including, Tau, Aβ, α-Syn (Apetz et al. 2014; Blanchard et al. 2004; Pithadia et al. 2016; Stefani and Rigacci 2013). Other polyphenolic compounds like morin hydrate, silibinin, quercetin, azadirachtin and salvianolic acid B have also been investigated as inhibitors of hIAPP aggregation (Cheng et al., 2012, 2013; Dubey et al. 2019; Zelus et al. 2012); however, the detailed mechanistic insights into the process remains elusive.

MYR is a polyphenolic flavanoid, commonly found in fruits (like *Syzygium cumini commonly known as Jamun*), nuts, berries, tea, and red wine (Gajera et al. 2017; Hiermann et al. 1998). Anti-inflammatory, anti-oxidant, anti-hypertensive, anti-cancer, and anti-diabetic activities have been reported for this compound (Supplementary Table S1) (Borde et al. 2011; Chang et al. 2007; Chhikara et al. 2018; Karker et al. 2016; Semwal et al. 2016; Wang et al. 2010). In an earlier study, MYR was demonstrated to have anti-amyloidogenic properties against Aβ and egg white lysozyme (Hamaguchi et al. 2009; He et al. 2014; Ono et al. 2003); however its effect on hIAPP aggregation and disaggregation is highly debated (Supplementary Table S1). While on one hand, Noor et al. concluded that MYR is not an effective inhibitor of hIAPP aggregation (Noor et al. 2012); another study by Zelus et al. provided evidence that MYR inhibits hIAPP fibrillization and protects the mammalian PC12 cells from hIAPP-mediated cytotoxicity (Supplementary Table S1) (Zelus et al. 2012). However, the mechanistic and detailed structural insights on how MYR inhibits hIAPP fibrillization were not clear from these investigations. Moreover, the influence of MYR on the pre-formed fibrils and aggregates has not yet been reported.

In the current study, using detailed biophysical and cellular assays, we aimed to investigate the anti-amyloidogenic and anti-diabetic potential of MYR by targeting the hIAPP aggregation pathway. Cellular experiments performed with the rat insulinoma cells–INS-1E, showed that MYR mediates protection against hIAPP--induced cytotoxicity via reduction of mitochondrial and cellular reactive oxygen species (ROS) levels; reduction in lipid peroxidation and the associated membrane permeability; and restoration of mitochondrial membrane potential (MMP). Indeed, MYR supplementation resulted in restoration of the GSIS from hIAPP exposed mouse pancreatic islets. In addition to this, molecular dynamics simulations studies performed with the hIAPP pentameric fibril model revealed three possible binding sites [namely, site-1 ("NNFGAILSS") site-2 ("FLVHS"), and site-3 ("NVGSNT")] for MYR on the hIAPP fibrils. Overall, our results suggest that MYR may act as a potential inhibitor for amyloidogenesis and hence, can be used as a dietary supplement for more effective management of T2DM and related amyloidogenic disorders.

Results

MYR inhibits the aggregation of hIAPP *in vitro*

hIAPP is known to form amyloidogenic aggregates and the formation of these aggregates can be monitored by thioflavin T (ThT) fluorescence spectroscopy. ThT is a commonly used probe that detects cross β-sheet rich amyloid fibrils wherein its quantum yield increases significantly upon binding to amyloid fibrils (Biancalana et al.

2009). In order to monitor the kinetics of hIAPP fibrillization in the presence of MYR, ThT fluorescence measurements were carried out. As can be seen from Figure 1A (Red), ThT fluorescence intensity of hIAPP increased with incubation time thereby demonstrating the formation of the cross-β sheet rich amyloid fibril. However, significant disruption in the amyloid formation was observed in samples where MYR supplementation was performed, thereby suggesting a strong inhibition of hIAPP aggregation (Figure 1A). In fact, MYR supplementation in as little as 1:0.5 M equivalents was enough to inhibit hIAPP aggregation completely (Figure 1A; green). We also investigated the effect of resveratrol supplementation on hIAPP aggregation as a positive control. Resveratrol exhibits anti-neuroinflammatory activity and is a known inhibitor of amyloidogenic proteins such as Aβ and hIAPP. Extensive work has been carried out previously to show the same (Sciacca et al. 2018; Sun et al. 2010; Tu et al. 2015). In line with the previous studies, we also observed an inhibitory action of resveratrol on hIAPP aggregation pathway (Figure S2).

Next, to validate these observations further and to eliminate the possibility that MYR was most likely competing for the same binding site as ThT on hIAPP, additional assays including intrinsic tyrosine (Y37) fluorescence measurements (to reveal the information about the changes in the structure and local environment) and 8-anilinonaphthalene-1-sulfonic acid (ANS) fluorescence spectroscopy were carried out. As expected, the intrinsic tyrosine fluorescence intensities for hIAPP alone increased significantly in a time-dependent manner (Figure 1B red, Figures S3 and S4). The maximum intensities were observed after 12 h of incubation at 37 °C; therefore, all further experiments were carried out in these conditions. MYR supplementation in 1:0.5 M equivalents (hIAPP:MYR) led to significant reduction in intrinsic tyrosine fluorescence intensities (Figure 1B, green), thus suggesting that an interaction between hIAPP and MYR exists. Fluorescence intensities further dropped when the molar equivalent was increased to 1:1 (Figure 1B, blue) and 1:5 (Figure 1B, pink). ANS fluorescence assays, used to probe changes in the exposed hydrophobic surfaces (carried out at 37 °C and 12 h incubation), also showed similar reduction in ANS fluorescence intensity, thereby suggesting towards a change in the hydrophobic surface of hIAPP upon interaction with MYR (Figure 1C).

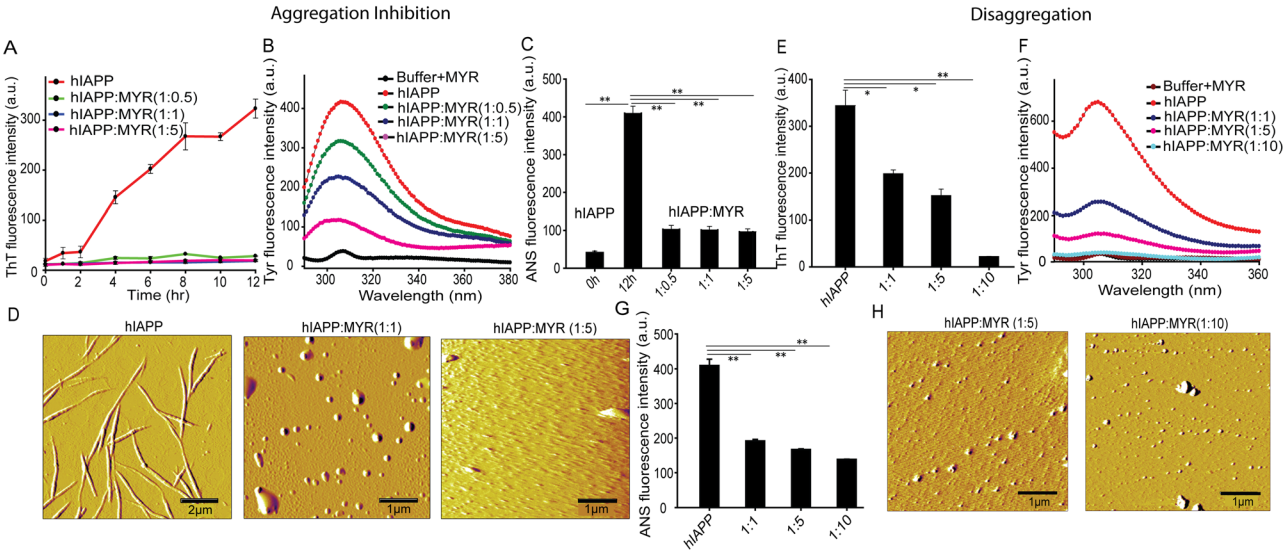

Figure 1: Myricetin (MYR) supplementation alters the amyloidogenicity of human islet amyloid polypeptide (hIAPP).
(A) Time dependent Thioflavin T fluorescence intensity of hIAPP with different molar ratio of MYR (hIAPP: MYR 1:0.5, 1:1 and 1:5); (B) Intrinsic tyrosine fluorescence intensity of hIAPP in presence of MYR at different concentration at 37 °C for 12 h; (C) Decrease in hydrophobic surface exposure of MYR supplemented hIAPP (in increasing concentrations) analysed by 8-anilinonaphthalene-1-sulfonic acid (ANS) fluorescence assay after incubation for 12 h at 37 °C; (D) Morphological study of hIAPP alone and in presence of MYR (1:1 and 1:5 respectively) by AFM imaging. Disaggregation of preformed hIAPP fibrils investigated by performing (E) Thioflavin T (ThT) fluorescence studies of hIAPP fibril alone and in presence of MYR in different molar equivalents (hIAPP: MYR = 1:1 and 1:5); and (F) Intrinsic tyrosine fluorescence measurement to assess the micro-environment of aromatic tyrosine residue of preformed hIAPP fibrils in presence of different molar equivalents of MYR; (G) ANS fluorescence measurements to assess the hydrophobic surface exposure of preformed hIAPP fibrils in the presence of different molar equivalents of MYR; (H) Representative AFM images of preformed hIAPP fibrils after incubation with different molar equivalents of MYR (hIAPP: MYR = 1:5 & 1:10). *$p < 0.05$, ** $p < 0.01$, ***$p < 0.001$, ****$p < 0.0001$.

Furthermore, atomic force microscopy (AFM) imaging of the hIAPP fibrils in the absence and in the presence of MYR was performed. As can be seen from Figure 1D and Figure S5A, mature and elongated fibrils were observed in the hIAPP samples. On the other hand, MYR supplementation (hIAPP:MYR = 1:1 & 1:5) clearly indicated the loss of fibrillar structure and the formation of amorphous aggregates (Figure 1D; Figure S5B and C). While MYR supplementation in 1:1 M equivalents resulted in the formation of globular aggregates; amorphous aggregates were observed when MYR was added in five fold molar excess (Figure 1D).

Myricetin disaggregates the preformed hIAPP fibrils *in vitro*

An alternative strategy for the management of T2DM would be to target the preformed hIAPP fibrils in the pancreatic β-islets. Therefore, we investigated the effect of MYR supplementation of the pre-formed hIAPP fibrils *in vitro*. Briefly, preformed hIAPP fibrils were incubated with different molar equivalents of MYR (hIAPP:MYR = 1:1, 1:5 and 1:10) for 1 h at room temperature and morphological and biophysical studies were carried out. ThT fluorescence assay showed a significant decrease in ThT fluorescence intensity of pre-existing hIAPP fibrils incubated with MYR in a dose dependent manner (Figure 1E). These studies were further validated by performing intrinsic Y37 fluorescence measurements wherein a significant reduction in the intrinsic tyrosine fluorescence intensity were observed for preformed hIAPP fibrils co-incubated with MYR when compared to the untreated hIAPP fibrils (Figure 1F). Since, Y37 is present at the C-terminal of the hIAPP peptide, these investigations also pointed out that one of the possible sites of MYR interaction with hIAPP probably lies around Y37. Furthermore, ANS fluorescence assay showed a significant reduction in ANS fluorescence intensity for MYR supplemented preformed hIAPP fibrils when compared to the fibrils alone (Figure 1G). These investigations suggested a change in the hydrophobic surface exposure in the hIAPP fibrils upon addition of MYR. Indeed, these findings were confirmed by AFM imaging to analyze the morphology of pre-formed hIAPP fibrils in the presence and absence of MYR (Figure 1H). The pre-formed hIAPP fibrils formed dense fibrillar network, characteristic of amyloidogenic proteins (Figure 1D). On the other hand, supplementation with MYR in 1:5 and 1:10 M equivalents resulted in the formation of smaller, amorphous hIAPP aggregates (Figure 1H; Figure S6B and C).

Secondary structure of hIAPP is affected in the presence of MYR

The pathway that leads to the formation of amyloidogenic aggregates and fibrils starts with the conversion of unstructured monomer to cross β-sheet rich amyloid fibrils via various intermediate stages (Buchanan et al. 2013). This involves several changes in the secondary structure of the peptide which can be monitored using far-UV CD spectroscopy and fourier transforms infrared (FTIR) spectroscopy studies. Figure 2A depicts the structural transitions that occur in hIAPP as it proceeds from a random coil structure (black) to typical β-sheet conformation (a major negative peak at 220 nm; red) via the formation of helical intermediates (blue and green) over the period of 12 h. On the other hand, the incubation of hIAPP with MYR (1:1 M equivalents) for as little as 4 h (blue) and 8 h (green) resulted in significant conformational changes. Indeed by 12 h, a completely helical conformation was observed for hIAPP supplemented with MYR, thereby indicating the complete absence of amyloid aggregates (Figure 2B; red). Similar structural transitions were observed when preformed hIAPP fibrils were co-incubated for 12 h with MYR in 1:5 (Purple) and 1:10 (Cyan) molar equivalents, respectively (Figure 2B). The quantification of secondary structure analysis has been summarized in Supplementary Table S2.

Similar structural transitions were observed in hIAPP peptides supplemented with MYR using FTIR spectroscopy. The recorded FTIR spectra were deconvoluted from the region between 1600 to 1800 cm^{-1} for all samples, and peaks were assigned according to published reports (Barth 2007). The spectra for hIAPP peptide showed a predominant band near 1632 cm^{-1} and 1696 cm^{-1}, thereby suggesting the presence of β-sheet, with a small amount of coil contents (1654 cm^{-1}) and β-turns (1676 cm^{-1}) (Figure 2C). The addition of equimolar amount of MYR (1:1 M ratio) resulted in conformational transition, which consisted majorly of α-helical contents (1648 cm^{-1}) with some β-sheet contents (1693 cm^{-1}) and β-turn (1668 and 1683 cm^{-1}) (Figure 2D).

MYR protects pancreatic β-cells against hIAPP-mediated cytotoxicity

Cytotoxicity mediated by hIAPP was investigated in INS-1E cells using the MTT and LDH release assays. In line with previous reports from our and other labs (Dubey et al. 2017; Hernández et al. 2018; Li et al. 2009), it was observed that synthetic hIAPP significantly affected the viability of INS-1E cells when compared to untreated

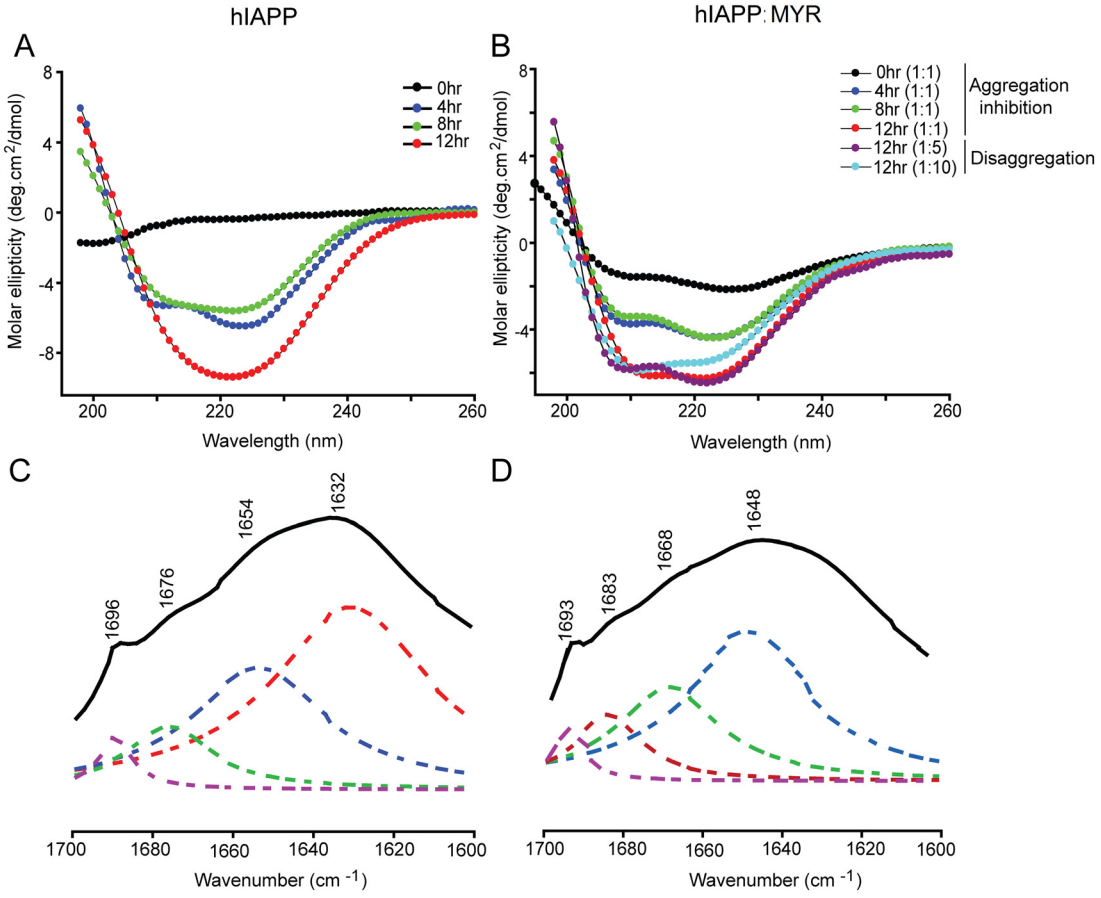

Figure 2: Structural characterization of hIAPP in presence of MYR. Far-UV CD spectra of (A) hIAPP alone and; (B) hIAPP and pre-formed hIAPP fibrils supplemented with equimolar concentration of MYR monitored at 0, 4, 8 and 12 h. FT-IR spectrum of (C) hIAPP alone and; (D) supplemented with equimolar concentration of MYR monitored after 12 h.

control cells in 24 h [Figure 3A (as assessed by MTT assay) and Figure 3B (as assessed by LDH release assay)]. However, supplementation of MYR in molar ratios as low as 1:1 mediated protection from hIAPP-induced cytotoxicity. Control experiments with MYR alone showed no significant effect on cellular viability at the tested concentrations (Figure S7). The compromised proliferation capacity of INS-1E in the presence of hIAPP was rescued by the supplementation of MYR in 1:5 M equivalents (Figure 3C). Likewise, co-incubation of the pre-formed hIAPP fibrils with MYR in 1:5 M equivalents protected INS-1E cells from hIAPP-mediated cytotoxicity (as assessed by MTT assay) (Figure 3D).

The cytotoxicity in INS-1E cells upon hIAPP exposure was mediated by apoptosis, as assessed using Annexin V/PI staining. As can be observed from Figure 3E, the percentage of cells undergoing apoptosis increased from 16.20% (±2.5%) in untreated cells to 47.93% (±5.13%) in hIAPP treated INS-1E cells ($p < 0.001$). This was rescued upon MYR supplementation (in 1:5 M excess) and the percentage of apoptotic cells was reduced to 25.67% (±1.98%). In addition to this, the arrest of INS-1E cells incubated with hIAPP in the S and G2/M phase of the cell cycle was restored upon MYR supplementation in 1:5 M ratios (Figure 3F; quantified in Figure 3G). MYR supplementation in INS-1E cells showed no significant differences in the cell cycle profile when compared to the control cells, thereby strengthening our previous observation that MYR is not cytotoxic to INS-1E cells.

Exposure of INS-1E cells to hIAPP has been associated with induction of oxidative stress (Borchi et al. 2014; Dubey et al. 2017; Zraika et al. 2009). ROS levels in INS-1E cells were measured using DCFH-DA (cellular ROS levels; Figure 4A) and Mitosox Red (mitochondrial ROS levels; Figure 4B) and were found to be elevated in INS-1E cells exposed to hIAPP. MYR supplementation not only rescued hIAPP-exposed INS-1E cells from total cellular ROS (Figure 4A), mitochondrial ROS (Figure 4B); but also prevented the associated lipid peroxidation and membrane damage (expressed as TBARS/mg protein) (Figure 4C). These cells possessed healthier mitochondria (measured using JC-1–an indicator of mitochondrial membrane

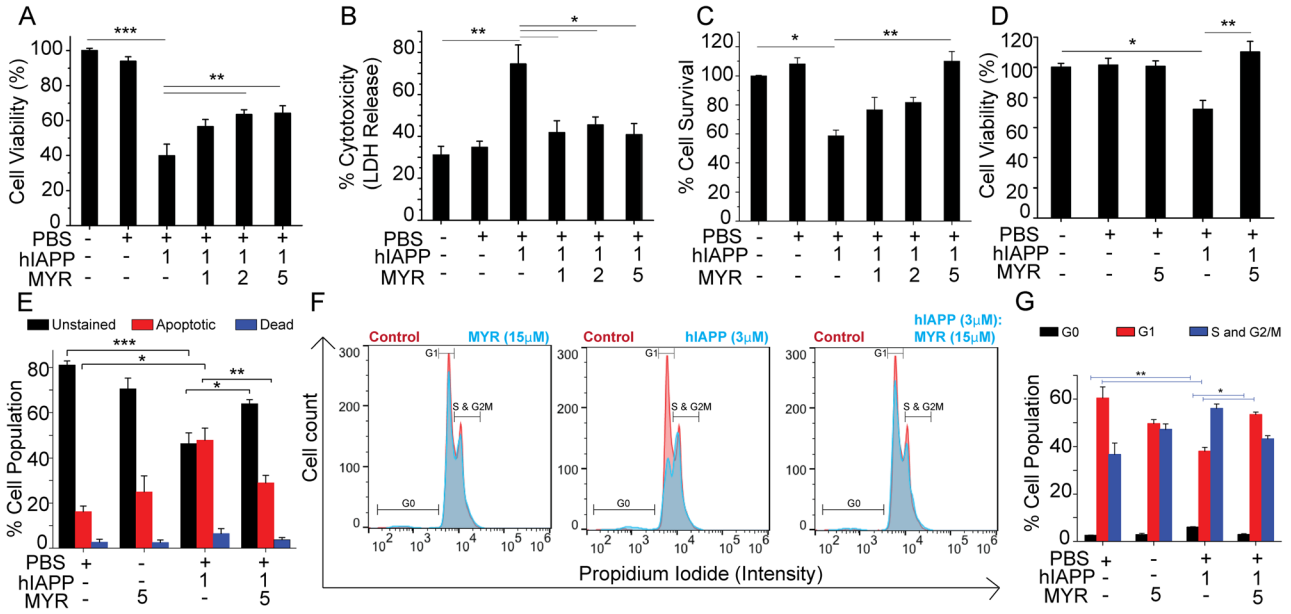

Figure 3: MYR mediates protection from hIAPP-induced cytotoxicity in INS-1E cells. Results from (A) MTT assay ($N = 4$), (B) LDH release assay ($N = 3$); and (C) Cellular proliferation capacity ($N = 3$) of hIAPP exposed INS-1E cells to measure the potential of MYR to prevent hIAPP aggregation. (D) MTT assay ($N = 3$) performed with pre-formed hIAPP fibrils to measure the potential of MYR to disaggregate preformed fibrils. (E) Quantitation of live, apoptotic and dead cells as assessed by the Annexin V-PI binding assay ($N = 3$). (F) Representative histograms depicting cell cycle profiles of INS-1E cells exposed to different experimental conditions. (G) Quantitation of cells in different phases of the cell cycle ($N = 3$). * $p < 0.05$, ** $p < 0.01$, ***$p < 0.001$.

potential), when compared to those exposed to hIAPP which showed depolarisation of MMP (depicted by an increase in population of JC-1 monomers that emit green fluorescence) (Figure 4D; quantified in Figure. 4E); had lesser DNA double strand breaks (measured by γ-H2AX stained foci–an indicator of DNA damage and apoptosis) when compared to hIAPP treated cells (Figure 4F); thereby pointing towards a protective role of MYR. Indeed, hIAPP treated cells stained positive with the amyloid specific probe – Thioflavin S (Figure 4G); on the other hand, this staining was significantly reduced in MYR supplemented hIAPP exposed INS-1E cells. Control cells and MYR alone treated cells did not show any significant staining for both γ-H2AX (Figure 4F)- and Thioflavin S (Figure 4G). Taken together, these results suggest that MYR protects pancreatic β-cells from hIAPP-induced cytotoxicity by decreasing oxidative stress, which, in turn, is associated with reduced lipid peroxidation, DNA damage; and restoration of the MMP.

MYR supplementation rescues the functional defects in hIAPP-exposed mouse pancreatic islets

In addition to inducing cytotoxicity, the formation of amyloidogenic aggregates of hIAPP in the pancreatic β-cells has been associated with a loss in their function, measured in terms of GSIS (Dubey et al. 2017). The isolated pancreatic islets were exposed to hIAPP alone and with MYR supplementation (1:5 M equivalents) for 24 h, and response to glucose was measured. As can be seen from Figure 4H, in the control islets, the amount of insulin release increased significantly from 71.41 ± 6.96 μIU/ml under basal glucose conditions to 120.01 ± 8.94 μIU/ml under glucose-stimulated conditions ($p < 0.01$; Figure 4H), thereby confirming the functionality of our isolated islets. On the other hand, hIAPP exposure to the isolated islets not only reduced the insulin release in response to basal glucose, but also affected the insulin release in response to stimulated glucose. In line with our previous results, it was observed that MYR supplementation restored the functional defect in hIAPP-exposed islets and restored the insulin secretion in response to basal and stimulates glucose conditions. MYR alone, however, did not affect the insulin release under basal and stimulated glucose conditions and was similar to that of control islets. Therefore, based on our biophysical and cellular results, we can conclude that MYR inhibits the formation of hIAPP toxic aggregates, mediates disaggregation of preformed aggregates and thus restores the viability and function of pancreatic β-cells.

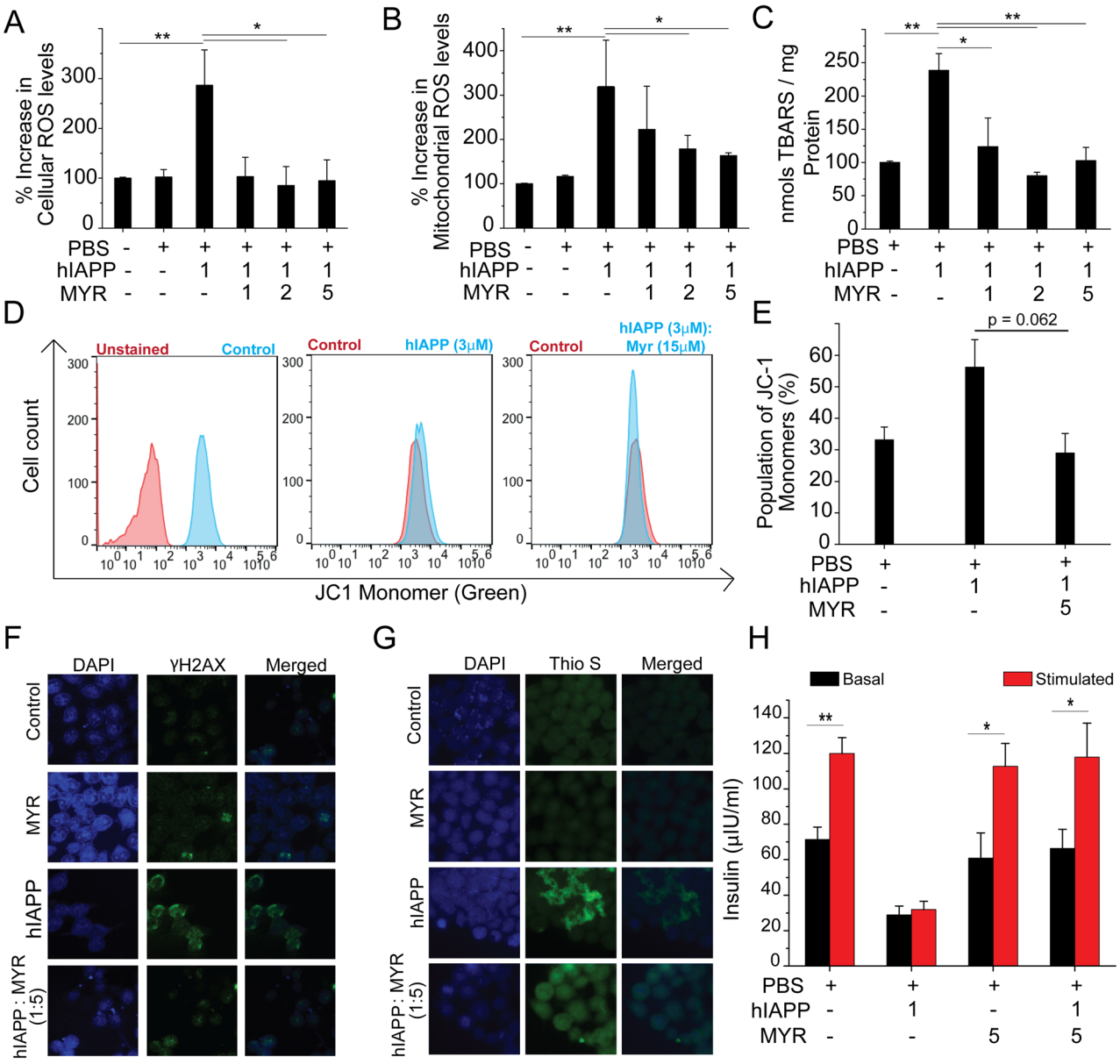

Figure 4: MYR mediates protection and restores dysfunction in pancreatic β-cells.
(A) Intracellular (measured using DCFH-DA; $N = 4$); and (B) mitochondrial reactive oxygen species (ROS) levels (measured using Mitosox Red; $N = 4$) in INS-1E cells exposed to hIAPP alone and/or in the presence of different molar equivalents of MYR. (C) Lipid peroxidation measured in terms of nmol of TBARs/mg protein ($N = 5$). (D) Representative histograms of JC-1 stained INS-1E cells exposed to different experimental conditions. (E) Quantitation of JC-1-stained cells ($N = 3$). (F) Reduced DNA damage (indicated by reduced γH2AX staining) in MYR supplemented hIAPP-treated cells ($N = 3$). (G) Thioflavin-S staining to visualize amyloid aggregates in INS-1E cells exposed to the different experimental conditions. (H) Results from glucose stimulated insulin secretion (GSIS) assay performed on isolated pancreatic islets exposed to hIAPP alone and/or in the presence of MYR showed significantly different insulin secretion in the GSIS assay ($N = 4$). *$p < 0.05$, **$p < 0.01$, ***$p < 0.001$.

MYR binds to hIAPP fibril

To identify the possible binding sites of MYR on hIAPP, three 350 ns long atomistic MD simulations were performed with the $hIAPP_{1-37}$ pentameric fibril model and MYR at molar ratio of 1:2 (hIAPP:MYR); and $hIAPP_{1-37}$ alone (i.e., apo-$hIAPP_{1-37}$) as control (Figure 5B). The initial ordered structure of pentameric fibril model seemed significantly distorted after binding of MYR (Figure 5). The planarity of the $hIAPP_{1-37}$ pentameric fibril model was monitored and it was noted that while apo-hIAPP showed single population at 180°, MYR-bound hIAPP showed additional populations at 30° and 120° (Figure 5G). We identified four binding sites for MYR on hIAPP based on the

contact frequency between MYR and hIAPP residues over the last 50 ns of the simulation data (Figure S8) i.e. site-1 ("NNFGAILSS") site-2 ("FLVHS"), site-3 ("NVGSNT"), and the C-terminus Y37 (Figure 5). We observed that MYR interacts with Y37 in all the three simulations, through aromatic π-π interaction (Figure 5F), in line with results obtained from tyrosine fluorescence measurement experiments. Thus, based on these results, it can be concluded that MYR has a great tendency to interact mainly at the C-terminus of the $hIAPP_{1-37}$ pentameric fibril model, which can be suggested as one of the core regions (amyloidogenic fragment) of amyloid formation in case of hIAPP.

Discussion

Human islet amyloid polypeptide (hIAPP) is the major component of the amyloid deposits found in the pancreatic islets of type 2 diabetic patients and plays a crucial role in the loss and dysfunction of insulin-secreting pancreatic β-cells (Cao et al. 2013). Most lifestyle and therapeutic interventions developed for the management of T2DM currently aim at delaying the progression of diabetic complications rather than reversing them (Chaudhury et al. 2017). Interestingly, there have been reports which indicate that the process of hIAPP fibrillization starts much before hyperglycemia sets in the system (Akter et al. 2016). Therefore, targeting hIAPP aggregation by development of molecules that inhibit amyloid formation hold a great potential for the earlier management of T2DM, much before than the disease actually sets in the system. In addition to this, identification of molecules that disaggregate the preformed fibrils would further aid in reversing β-cell dysfunction and help in more effective disease management. Along these lines, different classes of compounds

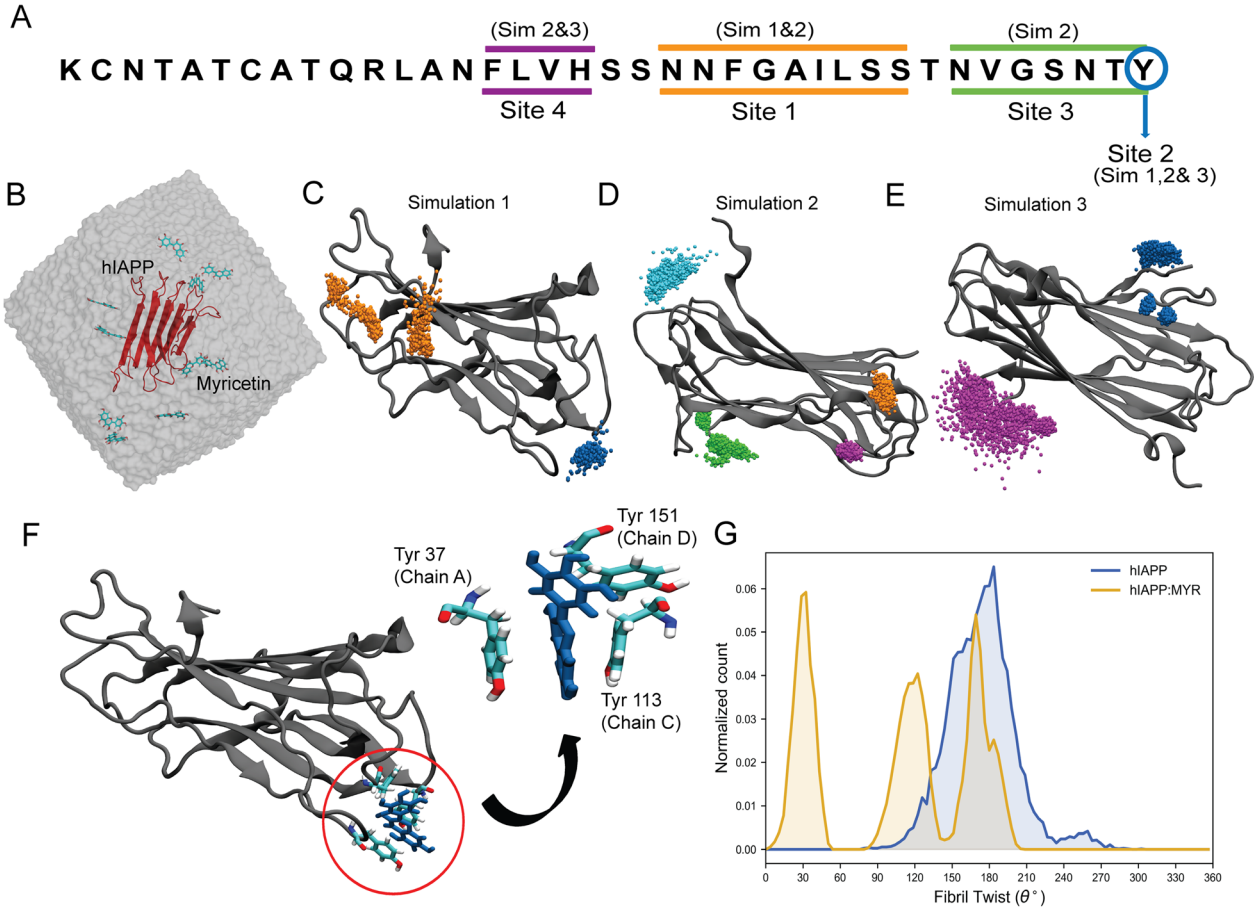

Figure 5: Binding distribution of MYR on $hIAPP_{1-37}$ pentameric model.
(A) Shows the summary of the binding positions of MYR on hIAPP over the three simulations performed. (B) Simulation box showing hIAPP pentamer (red) and the random positions of MYR in water (transparent grey). This was the starting configuration for all the three MYR bound hIAPP simulations. Four major binding sites were observed in the panels (C), (D) and (E). The four major binding sites of MYR to hIAPP pentamer (depicted in grey), in all the three independent simulations, are shown in orange, green, purple and blue colour. Panel (F) shows the interaction of MYR with tyrosine residue (Y37) of $hIAPP_{1-37}$ pentameric fibril model and the excerpt of this interaction is also shown in the inset. (G) Distribution of the fibril twist angles from hIAPP and hIAPP:MYR simulations.

have been identified that inhibit hIAPP fibrillization and thus reduce hIAPP-induced cytotoxicity in pancreatic β-cells (Brender et al. 2010; Cheng et al., 2012, 2013; He et al. 2013; Jiang et al. 2011).

Flavonoids and polyphenols form a major class of molecules (Patel et al. 2012) that are thought to interact with amyloidogenic core regions via aromatic π-π interactions and interfere with their self-assembly process thereby reducing aggregate formation (Sgarbossa 2012). Several polyphenolic compounds including EGCG, curcumin, resveratrol, ferulic acid (FA), etc. have been tested for their anti-diabetic potential by targeting hIAPP aggregation (Pithadia et al. 2016; Sciacca et al. 2018; Velander et al. 2016). Other polyphenolic compounds like morin hydrate, silibinin and salvianolic acid B were also studied as candidates that target hIAPP aggregation (Cheng et al., 2012, 2013; Noor et al. 2012). Nevertheless, most of these studies were performed *in vitro* wherein the mechanistic insights into the action of these inhibitors on hIAPP fibrillization remained elusive. Previous studies from our group identified Azadirachtin - a limonoid from Neem - as a potent inhibitor of hIAPP aggregation and were capable of disaggregating preformed fibrils (Dubey et al. 2017). Other studies also showed that EGCG and morin hydrate were also capable of disaggregating preexisting hIAPP fibrils.

Myricetin, a natural flavonoid, has been previously investigated for its hypoglycemic effect and hence has been proposed as an anti-diabetic and anti-amyloidogenic agent (Li and Ding 2012; Li et al. 2017) (Supplementary Table S1). Several studies have shown varying results on its potential to inhibit amyloid formation by Aβ peptide (Akaishi et al. 2008; Ono et al. 2003). A recent study showed that MYR potentially inhibits hIAPP aggregation and protects PC12 cells from hIAPP-mediated cytotoxicity (Zelus et al. 2012). In line with these observations, our study showed that MYR inhibited the formation of hIAPP aggregates *in vitro*, wherein the process was associated with changes in secondary structure (as measured by Far-UV CD and FT-IR measurements). Once it was confirmed by biophysical methods, we set out to gain mechanistic insights into process by which MYR mediates protection in pancreatic β-cells. Our results show that MYR not only inhibits the process of hIAPP aggregation *in vitro* in a dose-dependent manner; it also disaggregates the preformed hIAPP fibrils. Indeed, this is the first study that shows that MYR supplementation restores cellular viability in hIAPP exposed pancreatic β-cells by reduction of mitochondrial and cellular ROS levels; reduction in lipid peroxidation and the associated membrane permeability; and restoration of mitochondrial membrane potential (Figure 6). Indeed, results from Thio-S staining (*in vivo*) and AFM imaging (*in vitro*) clearly indicated that MYR supplementation inhibited the formation of hIAPP aggregates and converted them to amorphous off-pathway aggregates that are in turn non-toxic to pancreatic β-cells. Similar observations have also been reported earlier (Zelus et al. 2012). In addition to this, MYR supplementation also restored the functional defect in hIAPP-exposed pancreatic islets (as measure by GSIS assays). These results are in line with the previous

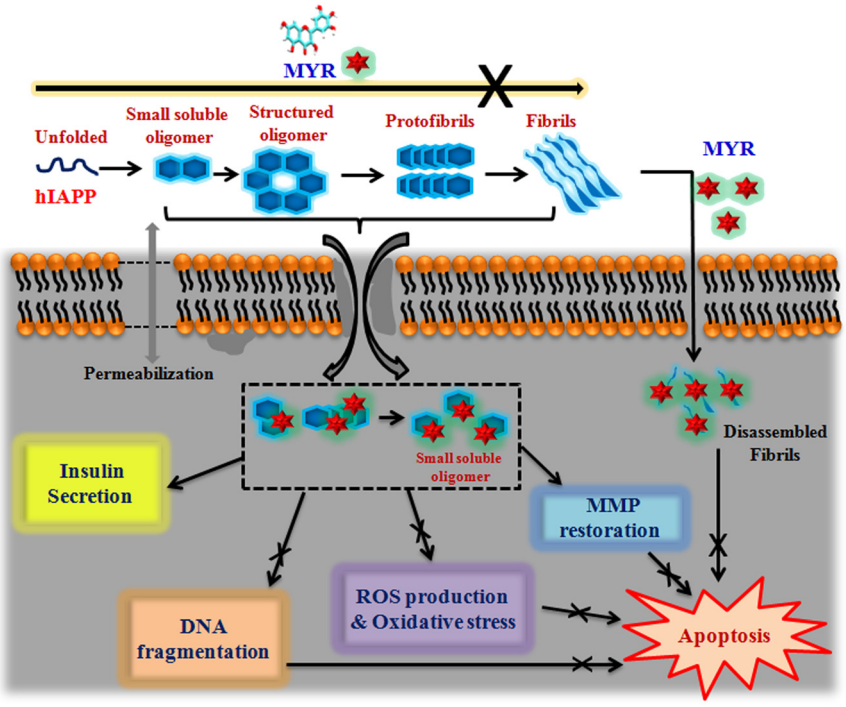

Figure 6: Schematic representation of effect of MYR on hIAPP fibrillization. hIAPP aggregates in a nucleation dependent pathway; wherein conversion of monomer to amyloid fibrils takes place via the formation of several intermediates. MYR inhibits the process of hIAPP aggregation, disaggregates pre-formed intracellular fibrils and in turn reduces ROS production, DNA damage and leads to restoration of mitochondrial membrane potential and insulin secretion potential. These eventually protect the pancreatic β-cells from undergoing apoptosis.

investigations that showed the anti-diabetic potential of MYR in rodent models of diabetes (Supplementary Table S1), thereby supporting our observations.

Intermolecular stacking interactions between aromatic residues in amyloidogenic peptides like hIAPP have been known to accelerate the self-assembly process thereby providing directionality and an prominent energetic contribution to the aggregation process (Gazit 2002; Sgarbossa 2012). Thus, aromatic-aromatic, as well as, aromatic-hydrophobic interactions have been proposed to play a significant role in the formation of hIAPP amyloid aggregated (Akter et al. 2016; Stanković et al. 2020; Tu and Raleigh 2013). Along these lines, the segments 8–20, 10–19, 20–29, and 30–37 have been identified as the amyloidogenic segments in hIAPP (Akter et al. 2016). In addition to this, aromatic amino acids – F15, F23 and Y37 have been shown to affect the aggregation process (Padrick and Miranker 2001) . Even though, a few earlier studies have hinted that $hIAPP_{18–20}$ oligomerisation starts from hexamers (Sun et al. 2010), the solid-state NMR derived pentameric structural model of hIAPP fibrils was used in the current study. This high-resolution structural model was best suited model used in all previous studies related to MD simulation of hIAPP fibrils. Moreover, no PDB ID was available for the hexameric model (as on August 2020).

Our MD data shows that MYR has tendency to bind at the amyloidogenic core region of the pentameric fibril model. This is consistent with our biophysical and cellular results. Based on the results obtained from biophysical, cellular and MD studies, we propose that interactions between MYR and F23 and the C-terminal Y37 residues of hIAPP might possibly block hIAPP oligomerization by interrupting the aromatic interactions during hIAPP self-assembly and thus converts them into off-pathway non-toxic aggregates. Additionally, MYR interaction with the pentameric fibril model appeared to twist the fibril axis. Such twists may disrupt the fibril growth and lead to off-pathway oligomers. A previous report from our lab have also identified Azadirachtin to mediate inhibition of hIAPP aggregation by interacting with amyloidogenic core region of hIAPP (Dubey et al. 2019).

In summary, we investigated the anti-amyloidogenic and anti-diabetic potential of MYR by targeting hIAPP aggregation pathway using a battery of biophysical, cellular and MD simulation studies. Our results show that MYR not only inhibits hIAPP aggregation, but also disaggregates pre-formed fibrils and protects pancreatic β-cells from hIAPP mediated cytotoxicity. MYR supplementation not only resulted in the reduction of both mitochondrial and intracellular ROS species, which in turn led to restoration of DNA damage, membrane damage, loss of MMP in hIAPP exposed β-cells; but also the functional defect by restoration of GSIS from pancreatic islets. Overall, our results suggest the MYR or its derivatives can be used for the effective management of T2DM and other amyloidogenic disorders.

Materials and methods

Materials

Synthetic hIAPP peptide (hIAPP) was purchased from Peptide 2.0 (Chantilly, VA). MYR, Resveratrol, dimethyl sulfoxide (DMSO), glucose solution (2.5 M), thiazolyl blue tetrazolium bromide (MTT), NaCl, bovine serum albumin (BSA), glycerol, methanol, tween-20, triton-X 100, propidium iodide (PI), Thioflavin S, and ANS were purchased from Sigma (St. Louis, MO, USA). Hexaflouroisopropanol (HFIP), ThT and lactate dehydrogenase kit were obtained from Himedia. Rabbit polyclonal anti-γH2AX antibodies were purchased from Abcam (Cambridge, UK). Goat anti-rabbit IgG were purchased from Novex. Nitrocellulose membrane was purchased from Biorad. Roswell Park Memorial Institute medium (RPMI-1640), 0.25% trypsin-EDTA solution, fetal bovine serum (FBS), Penicillin-streptomycin solution, phosphate buffered saline (PBS), 2′,7′-dichlorodihydrofluorescein diacetate (DCFHDA), MitoSOX Red, JC1 dye, and Annexin V/Dead cell apoptosis assay kit were purchased from Life Technologies (Carlsbad, CA). Mouse Insulin ELISA kit was purchased from Calbiotech. All other chemicals were of the highest grade available. All tissue culture ware was purchased from Corning. Chamber slides were purchased from Himedia.

Preparation of hIAPP, MYR and resveratrol

The lyophilized hIAPP peptide (Figure S1A) was dissolved in 100% hexaflouroisopropanol (HFIP) at 1 mM concentration, centrifuged to avoid the presence of any pre-formed aggregates and diluted with phosphate buffer (pH 7.4) to investigate its fibril and amyloid formation properties. Fresh solutions were prepared for each experiment. The stock solution of MYR (Figure S1B) was prepared by dissolving in water-DMSO (9:1) at room temperature, filtered through 0.2 μm to get clear solution and stored at 4 °C until further use. Resveratrol was prepared by dissolving in DMSO at room temperature and stored at 4 °C until further use.

Thioflavin T (ThT) fluorescence assay

The kinetics of fibril formation was monitored by the increase in fluorescence intensity of amyloid specific dye ThT (Biancalana and Koide 2010). Briefly, 20 μM of hIAPP peptide diluted in 10 mM phosphate buffer (20 mM NaH_2PO_4, 100 mM NaCl, 0.01% NaN_3 pH = 7.4) alone and in combination with different molar equivalents of MYR (hIAPP:MYR = 1:0.5, 1:1 and 1:5), and were incubated for increasing time intervals. Post-incubation, the samples were mixed with 5 μl of 1 mM ThT and incubated at room temperature for 30 min. The fluorescence spectra were recorded by exciting the samples at 450 nm and measuring

the emission spectra in the range of 460–500 nm on a spectrofluorimeter (Hitachi F-2500, Japan). The excitation and emission slit widths were kept at 5 nm. The emission values at 482 nm were plotted against increasing incubation time to study the kinetics of aggregation. Likewise, the disaggregation experiments were performed with 20 μM preformed hIAPP fibrils alone and in combination with different molar equivalents of MYR (hIAPP:MYR = 1:1, 1:5 and 1:10) for 12 h. The emission values at 482 nm thus obtained were plotted against the different experimental conditions used. Likewise, experiments were recorded with resveratrol which was used as a positive control.

ANS (8-anilinonaphthalene-1-sulfonate) fluorescence assay

In order to measure the changes in hydrophobicity, ANS fluorescence assay was performed. Briefly, 20 μM peptide sample [diluted in 10 mM phosphate buffer (pH 7.4)] alone and in combination with different molar equivalents of MYR (hIAPP:MYR = 1:1, 1:5 and 1:10) were incubated for 12 h. Post-incubation, the samples were mixed with 3 μl of 5 mM ANS dye and were further incubated at room temperature for 15 min in dark. The samples were excited at 370 nm and the emission spectra were recorded for 400–600 nm using a spectrofluorimeter (Hitachi F-2500, Japan). The excitation and emission slit widths were kept at 3 nm. Similar procedure was carried out for disaggregation study performed with 20 μM preformed hIAPP fibrils in presence of above mentioned molar equivalents of MYR for 12 h. The ANS fluorescence at 490 nm was plotted against the different experimental condition used.

Intrinsic tyrosine intrinsic fluorescence assay

To investigate the changes in the microenvironment around the aromatic residue–Y37, intrinsic tyrosine based fluorescence spectroscopy analysis was carried out. Briefly, 20 μM of diluted hIAPP peptide was incubated with different molar equivalents of MYR for 12 h at 37 °C. The samples were excited at 280 nm and the emission spectra were recorded for 290–400 nm using a spectrofluorimeter (Hitachi F-2500, Japan). The disaggregation of preformed hIAPP fibrils in presence of different molar equivalents of MYR (hIAPP: MYR 1:1, 1:5 and 1:10) were also performed in a similar manner.

Atomic force microscopy (AFM)

To visualise the effect of MYR supplementation on hIAPP fibrillization, AFM was performed (Asylum Research, CA, USA). Briefly, 40–50 μM of the diluted hIAPP peptide alone and in combination with different molar equivalents of MYR (hIAPP:MYR = 1:1 and 1:5) were incubation at 37 °C for 48 h. The samples were deposited on to freshly cleaved mica sheets, air-dried; washed twice with double distilled water; and were kept for drying at room temperature for around 40 min. Scanning was performed in tapping mode using Silicon nitride cantilever at a scan rate of 1 Hz. Random portions of the mica sheet were scanned to get desired images as well as to see the uniformity of the sample application. For the disaggregation study, the preformed fibrils were incubated with increasing molar equivalents of MYR (hIAPP:MYR = 1:5 and 1:10) for 1 h and the morphology of the fibrils was visualised as describe above.

Circular dichroism (CD) spectroscopy

Far-UV CD measurements were performed on a JASCO J-810 spectropolarimeter (JASCO, Japan) using a 0.1 cm path length cuvette (Hellma, Forest Hills, NY). Briefly, 20 μM samples of diluted hIAPP peptide alone and in presence of different molar equivalents of MYR (hIAPP:MYR = 1:1 and 1:5) were prepared and far-UV CD measurements were carried out. Likewise, the preformed hIAPP fibrils were incubated with MYR (hIAPP:MYR = 1:5 and 1:10) in 10 mM phosphate buffer (pH 7.4) and CD spectroscopy was carried out. All measurements were performed at 25 °C. Raw data were smoothened and measurements from the buffer were subtracted from that of the protein samples. The CD spectra have been represented as a plot of molar ellipticity (θ) in deg cm^2 $dmol^{-1}$ versus the wavelength. The secondary structure propensities obtained from the data were calculated using Jasco manager ver. 2.

Fourier transforms infrared (FTIR) spectroscopy

In order to measure the changes in the secondary structure of hIAPP in presence of MYR, FTIR spectroscopy was carried out. Briefly, 20 μM hIAPP peptide samples alone or in the presence of different molar equivalents (hIAPP:MYR = 1:1 and 1:5) were incubated for 12 h; spotted on potassium bromide (KBr) pellet; and dried immediately under IR lamp. The background spectra were recorded by spotting 10 μl buffer on the KBr pellet. Spectra in the region of 1600–1800 cm^{-1} were acquired as an average spectrum of 32 scans using a Vertex-80 FTIR system (Bruker, Germany). The spectra were subjected to Fourier self-deconvolution (FSD) of amide I region (1600–1700 cm^{-1}), followed by Lorentzian curve fitting using Opus 65 software (Bruker, Germany).

Cell culture

INS-1E cells, obtained as a kind gift from Prof. Claes Wollheim and Prof. Pierre Machler (University of Geneva Medical Center, Switzerland), between passages 56 and 65 were used for the study. Cells were grown in monolayer cultures in a humidified 5% CO_2 atmosphere at 37 °C in RPMI 1640 media (Life Technologies) supplemented with 10 mM HEPES, 1 mM pyruvate, 50 μM 2-mercaptoethanol, 10% (v/v) heat inactivated FBS, 100 units/ml penicillin and 100 μg/ml streptomycin (Merglen et al. 2004).

Cellular viability assays

The effect of hIAPP exposure on cellular viability in INS-1E cells at 24 h was investigated using the MTT assay and the Lactate Dehydrogenase (LDH) release assay (Himedia), as described earlier (Dubey et al. 2019). Untreated wells containing only cells in culture media and those treated with PBS were evaluated as controls. The reduction in cell viability as measured by the MTT assay was expressed as a percentage for each condition relative to control set (set at 100%). On the other

hand, results from the LDH release assay were expressed in terms of % cytotoxicity as per the formula below:

$$\%\,Cytotoxicity = \frac{Treated\,LDH\,activity - Spontaneous\,LDH\,activity}{Maximum\,LDH\,activity - Spontaneous\,LDH\,activity} \times 100$$

Apoptosis assay and cell cycle analysis

Flow cytometry was performed using the Annexin V-FITC apoptosis detection kit (Invitrogen, USA) for estimation of apoptotic and dead populations as described (Dubey et al. 2019). Cell cycle analysis was carried out by flow cytometry as described (Dubey et al. 2017). Ten thousand cells were analyzed for each sample. Unstained cells (without Annexin-V-FITC and PI) were used as a control and single stained cells (Annexin V-FITC or PI positive) were used for fluorescence compensation. Samples were acquired on Attune NxT flow cytometer (ThermoFisher Scientific) and analyzed using Attune NxT Flow Cytometer Software (ThermoFisher Scientific).

Reactive oxygen species (ROS) measurement

ROS levels were assessed by incubating INS-1E cells with either DCF-DA (10 μmol) or MitoSox (5 μmol) for 30 min at 37 °C (Dubey et al. 2019). The data was normalized with respect to the number of viable cells (as determined by the MTT assay).

Lipid peroxidation

Lipid peroxidation was determined in *INS-1E* cells as describe earlier (Dubey et al. 2019). Tetramethoxy propane was used as a standard. Fluorescence was measured at excitation 485 nm and emission 535 nm. The amount of protein was quantitated using BCA reagent and the results were expressed as nmol TBARS/mg protein.

Immunofluorescence

INS-1E cells were grown on cover slips in 6-well plates, treated with 5 μM hIAPP, 25 μM MYR (5 M equivalents) and the 1:5 combination mixture of hIAPP:MYR (5 μM:25 μM) for another 24 h. Post-incubation, the cells were fixed and stained with Thioflavin S and γH2AX. The coverslips were mounted onto slides with Vectashield antifade mountant containing DAPI (Vector Laboratories). Imaging was performed on a fluorescent microscope (Leica DM3000 LED) and the images were processed using Application Suite X (Leica).

Mitochondrial membrane potential (MMP) measurement

MMP was assessed in INS-1E cells using JC-1 dye (ThermoFisher Scientific) as described (Dubey et al. 2019). JC-1 stained cells were acquired using Attune NxT flow cytometer (ThermoFisher Scientific) and analyzed using Attune NxT Flow Cytometer Software (ThermoFisher Scientific). An increased ratio of J-monomers (emit green fluorescence at 490 nm in depolarized mitochondria) and a shift in the green fluorescence indicates mitochondrial damage.

Pancreatic islets isolation and glucose-stimulated insulin secretion (GSIS) assay

Eight to 10-week-old CD1 mice housed in polypropylene cages at 25 ± 2 °C under a standard 12 h light/dark cycle and were provided with animal feed and water *ad libitum*. Research was conducted in accordance with the guidelines of the Committee for the purpose of Control and Supervision of Experiments on Animals (CPCSEA) and the study protocol was approved by the Institutional Animal Ethics Committee (IAEC) at IISER-Pune, Pune constituted as per the guidelines provided by the Committee for the purpose of control and supervision of experiments on animals (CPCSEA), Government of India.

Pancreatic islets were isolated from these mice as described (Dubey et al. 2017). The isolated islets were treated with freshly sonicated hIAPP fibrils in the presence/absence of different molar equivalents of MYR for 24 h. Following this incubation, GSIS assay was performed to access the functionality of islets as described (Dubey et al. 2017) using Mouse insulin ELISA kit (Calbiotech). GSIS was expressed as the fold increase in insulin secretion under stimulated conditions–calculated by taking the ratio of insulin secreted under stimulated glucose conditions to insulin secreted under basal glucose conditions.

Molecular dynamics (MD) simulation

Co-ordinates of the $hIAPP_{1-37}$ pentameric fibril model were provided as a kind gift from Prof. R. Tycko (NIH, USA). To generate generalized amber forcefield parameters for MYR, geometry of MYR was optimized using Gaussian 03 package (Frisch et al. 2009) with HF/6–31g* basis set (Coulson 1938; Ochterski et al. 1996; Petersson et al. 1988) followed by calculation of mulliken population analysis using HF/6–31g* basis set (Besler et al. 1990; Singh and Kollman 1984). Ambertools12 was used to generate the GAFF forcefield parameters which were converted to GROMACS compatible format using amb2gmx.pl script. All simulations were performed with GROMACS4.6 package and amber99sb forcefield (Berendsen et al. 1995; Lee et al. 2016; Van Der Spoel et al. 2005) was used for hIAPP. hIAPP was placed in a dodecahedron box with 1 nm distance between the protein and the box walls. Two protein systems were simulated; apo hIAPP, and hIAPP with MYR at 1:2 ratio (hIAPP:MYR = 1:2). For hIAPP:MYR, five MYR molecules were placed at random positions. Both the simulation systems were solvated with TIP3P (Mahoney and Jorgensen 2000) water and neutralized using Na^+–Cl^- ions. The entire system was energy minimized followed by temperature and pressure equilibration as per the protocol described elsewhere (Dantu et al. 2017). Three independent production run simulations were performed, each 350 ns long to collect data at 40 ps intervals for data analysis. Simulation data was analysed using GROMACS tools, in-house python scripts and residue contacts were analysed using g_contacts tool (Blau and Grubmuller 2013).

Statistical analysis

All results have been presented as mean ± SEM. Statistical analysis was performed by one-way ANOVA and Tukey HSD post hoc test; a value of $p < 0.05$ was considered to be a significant difference between groups.

Acknowledgments: The authors acknowledge Bio-AFM facility funded by RFIC-IIT Bombay; Central instrumentation facility at Savitribai Phule Pune University (SPPU); and the flow cytometer facility at Institute of Applied Biology Research and Development, Pune. We thank the staff of the National Facility for Gene Function in Health and Disease (NFGFHD) at IISER-Pune for technical support. R.D. is thankful for financial assistance from UGC-JRF, Government of India. R.P. acknowledges financial assistance from MHRD, Government of India. A.K. acknowledges funding from CSIR (RD/0111-CSIR000-016) Government of India and IIT Bombay Seed grant (11IRCCSG003). S.S. acknowledges funding from Ramalingaswami fellowship (BT/RLF/Re-entry/11/2012; Department of Biotechnology-DBT, Government of India); and University Grants Commission (UGC), Government of India F.4-5(18-FRP) (IV-Cycle)/2017(BSR)). The S.S. laboratory has been generously supported by Board of College and University Development (BCUD) grant (SPPU); Research and Development grant to the Department of Biotechnology, SPPU; and UPE Phase II grant, and RUSA 2.0 to SPPU. S.H.K. acknowledges DBT, GOI for her Master in Biotechnology fellowship and DMS acknowledges financial assistance from DBT-JRF, Government of India. J.D.A. acknowledges the funding from Start-Up Research Grant by Science and Engineering Research Board (SB/YS/LS-23/2014; SERB), Government of India. INS-1E cells were obtained as a kind gift from Prof. Claes Wollheim and Prof. Pierre Machler, University of Geneva Medical Centre. We are also very thankful to Professor Robert Tycko, NIH, for providing the pentameric coordinates of hIAPP for the molecular dynamics study.

Author contribution: AK, RD & SS conceived and designed the experiments. RD, SHK, RP, DMS, JDA and SS performed the experiment. RD, SHK, DMS, JDA, SS and AK were involved in analysis and interpretation of data. SCD performed MD simulation study. NM performed the AFM imaging experiments. JC, SS and AK contributed regents/materials/analysis tools. RD, SCD, SHK, DMS, JDA, SS and AK compiled the data. RD, SCD, JDA, JC, SS and AK wrote the manuscript. All the authors have accepted responsibility for the entire content of this submitted manuscript and approved submission.

Research funding: Council of Scientific and industrial research, Government of India (RD/0111-CSIR000-016) and Indian Institute of Technology, Bombay (11IRCCSG003); Wadhwani Research Center of Bioengineering (RD/018/-DONWR04-001/); Ramalingaswami fellowship (BT/RLF/Re-entry/11/2012; Department of Biotechnology-DBT, Government of India); and University Grants Commission (UGC, Government of India F.4-5(18-FRP) (IV-Cycle)/2017(BSR))

Conflict of interest statement: The authors declare that they have no conflicts of interest with the contents of this article.

References

Akaishi, T., Morimoto, T., Shibao, M., Watanabe, S., Sakai-Kato, K., Utsunomiya-Tate, N., and Abe, K. (2008). Structural requirements for the flavonoid fisetin in inhibiting fibril formation of amyloid β protein. Neurosci. Lett. 444: 280–285.

Akter, R., Cao, P., Noor, H., Ridgway, Z., Tu, L.H., Wang, H., Wong, A.G., Zhang, X., Abedini, A., Schmidt, A.M., et al. (2016). Islet amyloid polypeptide: structure, function, and pathophysiology. J. Diabetes Res. 2016: 1–18.

Apetz, N., Munch, G., Govindaraghavan, S., and Gyengesi, E. (2014). Natural compounds and plant extracts as therapeutics against chronic inflammation in Alzheimer's disease–a translational perspective. CNS Neurol. Disord. Drug Targets 13: 1175–1191.

Barth, A. (2007). Infrared spectroscopy of proteins. Biochim. Biophys. Acta Bioenerg. 1767: 1073–1101.

Berendsen, H.J., van der Spoel, D., and van Drunen, R. (1995). GROMACS: a message-passing parallel molecular dynamics implementation. Comput. Phys. Commun. 91: 43–56.

Besler, B.H., Merz, K.M., Jr., and Kollman, P.A. (1990). Atomic charges derived from semiempirical methods. J. Comput. Chem. 11: 431–439.

Biancalana, M. and Koide, S. (2010). Molecular mechanism of Thioflavin-T binding to amyloid fibrils. Biochim. Biophys. Acta Proteins Proteomics 1804: 1405–1412.

Biancalana, M., Makabe, K., Koide, A., and Koide, S. (2009). Molecular mechanism of thioflavin-T binding to the surface of β-rich peptide self-assemblies. J. Mol. Biol. 385: 1052–1063.

Blanchard, B.J., Chen, A., Rozeboom, L.M., Stafford, K.A., Weigele, P., and Ingram, V.M. (2004). Efficient reversal of Alzheimer's disease fibril formation and elimination of neurotoxicity by a small molecule. Proc. Natl. Acad. Sci. U. S. A. 101: 14326–14332.

Blau, C. and Grubmuller, H. (2013). g_contacts: fast contact search in bio-molecular ensemble data. Comput. Phys. Commun. 184: 2856–2859.

Borchi, E., Bargelli, V., Guidotti, V., Berti, A., Stefani, M., Nediani, C., and Rigacci, S. (2014). Mild exposure of RIN-5F β-cells to human islet amyloid polypeptide aggregates upregulates antioxidant enzymes via NADPH oxidase-RAGE: an hormetic stimulus. Redox Biol. 2: 114–122.

Borde, P., Mohan, M., and Kasture, S. (2011). Effect of myricetin on deoxycorticosterone acetate (DOCA)-salt-hypertensive rats. Nat. Prod. Res. 25: 1549–1559.

Brender, J.R., Hartman, K., Nanga, R.P.R., Popovych, N., de la Salud Bea, R., Vivekanandan, S., Marsh, E.N.G., and Ramamoorthy, A. (2010). Role of zinc in human islet amyloid polypeptide aggregation. J. Am. Chem. Soc. 132: 8973–8983.

Buchanan, L.E., Dunkelberger, E.B., Tran, H.Q., Cheng, P.N., Chiu, C.C., Cao, P., Raleigh, D.P., De Pablo, J.J., Nowick, J.S., and Zanni, M.T. (2013). Mechanism of IAPP amyloid fibril formation involves an intermediate with a transient β-sheet. Proc. Natl. Acad. Sci. U. S. A. 110: 19285–19290.

Cadavez, L., Montane, J., Alcarraz-Vizán, G., Visa, M., Vidal-Fàbrega, L., Servitja, J.M., and Novials, A. (2014). Chaperones ameliorate beta cell dysfunction associated with human islet amyloid polypeptide overexpression. PLoS One 9: e101797.

Cao, P., Marek, P., Noor, H., Patsalo, V., Tu, L.H., Wang, H., Abedini, A., and Raleigh, D.P. (2013). Islet amyloid: from fundamental. FEBS Lett. 587: 1106–1118.

Chang, H., Mi, M.T., Gu, Y.Y., Yuan, J.L., Ling, W.H., and Lin, H. (2007). Effects of flavonoids with different structures on proliferation of leukemia cell line HL-60. Ai zheng = Aizheng = Chin. J. Cancer 26: 1309–1314.

Chaudhury, A., Duvoor, C., Reddy Dendi, V.S., Kraleti, S., Chada, A., Ravilla, R., Marco, A., Shekhawat, N.S., Montales, M.T., Kuriakose, K., et al. (2017). Clinical review of antidiabetic drugs: implications for type 2 diabetes mellitus management. Front. Endocrinol. 8: 6.

Cheng, B., Gong, H., Li, X., Sun, Y., Zhang, X., Chen, H., Liu, X., Zheng, L., and Huang, K. (2012). Silibinin inhibits the toxic aggregation of human islet amyloid polypeptide. Biochem. Biophys. Res. Commun. 419: 495–499.

Cheng, B., Gong, H., Li, X., Sun, Y., Chen, H., Zhang, X., Wu, Q., Zheng, L., and Huang, K. (2013). Salvianolic acid B inhibits the amyloid formation of human islet amyloid polypeptide and protects pancreatic beta-cells against cytotoxicity. Proteins Struct. Funct. Bioinf. 81: 613–621.

Chhikara, N., Kaur, R., Jaglan, S., Sharma, P., Gat, Y., and Panghal, A. (2018). Bioactive compounds and pharmacological and food applications of Syzygium cumini–a review. Food Funct. 9: 6096–6115.

Cooper, G.J., Leighton, B., Dimitriadis, G.D., Parry-Billings, M., Kowalchuk, J.M., Howland, K., Rothbard, J.B., Willis, A.C., and Reid, K.B. (1988). Amylin found in amyloid deposits in human type 2 diabetes mellitus may be a hormone that regulates glycogen metabolism in skeletal muscle. Proc. Natl. Acad. Sci. U. S. A. 85: 7763–7766.

Coulson, C.A. (1938). Self-consistent field for molecular hydrogen. Math. Proc. Camb. Philos. Soc. 34: 204–212.

Dantu, S.C., Khavnekar, S., and Kale, A. (2017). Conformational dynamics of Peb4 exhibit "mother's arms" chain model: a molecular dynamics study. J. Biomol. Struct. Dyn. 35: 2186–2196.

Dobson, C.M. (2003). Protein folding and misfolding. Nature 426: 884–890.

Dubey, R., Minj, P., Malik, N., Sardesai, D.M., Kulkarni, S.H., Acharya, J.D., Bhavesh, N.S., Sharma, S., and Kumar, A. (2017). Recombinant human islet amyloid polypeptide forms shorter fibrils and mediates β-cell apoptosis via generation of oxidative stress. Biochem. J. 474: 3915–3934.

Dubey, R., Patil, K., Dantu, S.C., Sardesai, D.M., Bhatia, P., Malik, N., Acharya, J.D., Sarkar, S., Ghosh, S., Chakrabarti, R., et al. (2019). Azadirachtin inhibits amyloid formation, disaggregates preformed fibrils and protects pancreatic β-cells from human islet amyloid polypeptide/amylin-induced cytotoxicity. Biochem. J. 476: 889–907.

Fernández-Gómez, I., Sablón-Carrazana, M., Bencomo-Martínez, A., Domínguez, G., Lara-Martínez, R., Altamirano-Bustamante, N.F., Jiménez-García, L.F., Pasten-Hidalgo, K., Castillo-Rodríguez, R.A., Altamirano, P., et al. (2018). Diabetes drug discovery: hIAPP1–37 polymorphic amyloid structures as novel therapeutic targets. Molecules 23: 686.

Frieden, C. (2007). Protein aggregation processes: in search of the mechanism. Protein Sci. 16: 2334–2344.

Frisch, M.J., Trucks, G.W., Schlegel, H.B., Scuseria, G.E., Robb, M.A., Cheeseman, J.R., Scalmani, G., Barone, V., Mennucci, B., Petersson, G.A., et al. (2009). *Gaussian 09, Revision A.1*, Vol. 121. Gaussian. Inc., Wallingford CT, pp. 150–166.

Gajera, H.P., Gevariya, S.N., Hirpara, D.G., Patel, S.V., and Golakiya, B.A. (2017). Antidiabetic and antioxidant functionality associated with phenolic constituents from fruit parts of indigenous black jamun (Syzygium cumini L.) landraces. J. Food Sci. Technol. 54: 3180–3191.

Gazit, E. (2002). A possible role for π-stacking in the self-assembly of amyloid fibrils. FASEB. J. 16: 77–83.

Hamaguchi, T., Ono, K., Murase, A., and Yamada, M. (2009). Phenolic compounds prevent Alzheimer's pathology through different effects on the amyloid-β aggregation pathway. Am. J. Pathol. 175: 2557–2565.

He, L., Wang, X., Zhao, C., Wang, H., and Du, W. (2013). Ruthenium complexes as novel inhibitors of human islet amyloid polypeptide fibril formation. Metallomics 5: 1599–1603.

He, J., Wang, Y., Chang, A.K., Xu, L., Wang, N., Chong, X., Li, H., Zhang, B., Jones, G.W., and Song, Y. (2014). Myricetin prevents fibrillogenesis of hen egg white lysozyme. J. Agric. Food Chem. 62: 9442–9449.

Hernández, M.G., Aguilar, A.G., Burillo, J., Oca, R.G., Manca, M.A., Novials, A., Alcarraz-Vizan, G., Guillén, C., and Benito, M. (2018). Pancreatic β cells overexpressing hIAPP impaired mitophagy and unbalanced mitochondrial dynamics. Cell Death Dis. 9: 1–11.

Hiermann, A., Schramm, H.W., and Laufer, S. (1998). Anti-inflammatory activity of myricetin-3-O-β-D-glucuronide and related compounds. Inflamm. Res. 47: 421–427.

Jayakanthan, K., Mohan, S., and Pinto, B.M. (2009). Structure proof and synthesis of kotalanol and de-O-sulfonated kotalanol, glycosidase inhibitors isolated from an herbal remedy for the treatment of type-2 diabetes. J. Am. Chem. Soc. 131: 5621–5626.

Jiang, P., Li, W., Shea, J.E., and Mu, Y. (2011). Resveratrol inhibits the formation of multiple-layered β-sheet oligomers of the human islet amyloid polypeptide segment 22–27. Biophys. J. 100: 1550–1558.

Jurgens, C.A., Toukatly, M.N., Fligner, C.L., Udayasankar, J., Subramanian, S.L., Zraika, S., Aston-Mourney, K., Carr, D.B., Westermark, P., Westermark, G.T., et al. (2011). β-cell loss and β-cell apoptosis in human type 2 diabetes are related to islet amyloid deposition. Am. J. Pathol. 178: 2632–2640.

Karker, M., Falleh, H., Msaada, K., Smaoui, A., Abdelly, C., Legault, J., and Ksouri, R. (2016). Antioxidant, anti-inflammatory and anticancer activities of the medicinal halophyte Reaumuria vermiculata. Excli Journal 15: 297–307.

Kusakabe, T., Ebihara, K., Sakai, T., Miyamoto, L., Aotani, D., Yamamoto, Y., Yamamoto-Kataoka, S., Aizawa-Abe, M., Fujikura, J., Hosoda, K., et al. (2012). Amylin improves the effect of leptin on insulin sensitivity in leptin-resistant diet-induced obese mice. Am. J. Physiol. Endocrinol. Metab. 302: E924–E931.

Lee, J., Cheng, X., Swails, J.M., Yeom, M.S., Eastman, P.K., Lemkul, J.A., Wei, S., Buckner, J., Jeong, J.C., Qi, Y., et al. (2016). CHARMM-GUI input generator for NAMD, GROMACS, AMBER, OpenMM, and CHARMM/OpenMM simulations using the

CHARMM36 additive force field. J. Chem. Theory Comput. 12: 405–413.

Li, Y. and Ding, Y. (2012). Minireview: therapeutic potential of myricetin in diabetes mellitus. Food Sci. Hum. Well. 1: 19–25.

Li, X.L., Xu, G., Chen, T., Wong, Y.S., Zhao, H.L., Fan, R.R., Gu, X.M., Tong, P.C., and Chan, J.C. (2009). Phycocyanin protects INS-1E pancreatic beta cells against human islet amyloid polypeptide-induced apoptosis through attenuating oxidative stress and modulating JNK and p38 mitogen-activated protein kinase pathways. Int. J. Biochem. Cell Biol. 41: 1526–1535.

Li, J., Guan, M., Li, C., Lyv, F., Zeng, Y., Zheng, Z., Wang, C., and Xue, Y. (2014). The dipeptidyl peptidase-4 inhibitor sitagliptin protects against dyslipidemia-related kidney injury in apolipoprotein E knockout mice. Int. J. Mol. Sci. 15: 11416–11434.

Li, Y., Zheng, X., Yi, X., Liu, C., Kong, D., Zhang, J., and Gong, M. (2017). Myricetin: a potent approach for the treatment of type 2 diabetes as a natural class B GPCR agonist. FASEB. J. 31: 2603–2611.

Ma, L., Li, X., Wang, Y., Zheng, W., and Chen, T. (2014). Cu (II) inhibits hIAPP fibrillation and promotes hIAPP-induced beta cell apoptosis through induction of ROS-mediated mitochondrial dysfunction. J. Inorg. Biochem. 140: 143–152.

Mahoney, M.W. and Jorgensen, W.L. (2000). A five-site model for liquid water and the reproduction of the density anomaly by rigid, nonpolarizable potential functions. J. Chem. Phys. 112: 8910–8922.

Marzban, L., Park, K., and Verchere, C.B. (2003). Islet amyloid polypeptide and type 2 diabetes. Exp. Gerontol. 38: 347–351.

Merglen, A., Theander, S., Rubi, B., Chaffard, G., Wollheim, C.B., and Maechler, P. (2004). Glucose sensitivity and metabolism-secretion coupling studied during two-year continuous culture in INS-1E insulinoma cells. Endocrinology 145: 667–678.

Mukherjee, A., Morales-Scheihing, D., Butler, P.C., and Soto, C. (2015). Type 2 diabetes as a protein misfolding disease. Trends Mol. Med. 21: 439–449.

Noor, H., Cao, P., and Raleigh, D.P. (2012). Morin hydrate inhibits amyloid formation by islet amyloid polypeptide and disaggregates amyloid fibers. Protein Sci. 21: 373–382.

Ochterski, J.W., Petersson, G.A., and Montgomery, J.A., Jr. (1996). A complete basis set model chemistry. V. Extensions to six or more heavy atoms. J. Chem. Phys. 104: 2598–2619.

Okada, A.K., Teranishi, K., Isas, J.M., Bedrood, S., Chow, R.H., and Langen, R. (2016). Diabetic risk factors promote islet amyloid polypeptide misfolding by a common, membrane-mediated mechanism. Sci. Rep. 6: 1–10.

Ono, K., Yoshiike, Y., Takashima, A., Hasegawa, K., Naiki, H., and Yamada, M. (2003). Potent anti-amyloidogenic and fibril-destabilizing effects of polyphenols in vitro: implications for the prevention and therapeutics of Alzheimer's disease. J. Neurochem. 87: 172–181.

Padrick, S.B. and Miranker, A.D. (2001). Islet amyloid polypeptide: identification of long-range contacts and local order on the fibrillogenesis pathway. J. Mol. Biol. 308: 783–794.

Patel, D.K., Prasad, S.K., Kumar, R., and Hemalatha, S. (2012). An overview on antidiabetic medicinal plants having insulin mimetic property. Asian Pac. J. Trop. Biomed. 2: 320–330.

Petersson, A., Bennett, A., Tensfeldt, T.G., Al-Laham, M.A., Shirley, W.A., and Mantzaris, J. (1988). A complete basis set model chemistry. I. The total energies of closed-shell atoms and hydrides of the first-row elements. J. Chem. Phys. 89: 2193–2218.

Pilkington, E.H., Gurzov, E.N., Kakinen, A., Litwak, S.A., Stanley, W.J., Davis, T.P., and Ke, P.C. (2016). Pancreatic β-cell membrane fluidity and toxicity induced by human islet amyloid polypeptide species. Sci. Rep. 6: 21274.

Pithadia, A., Brender, J.R., Fierke, C.A., and Ramamoorthy, A. (2016). Inhibition of IAPP aggregation and toxicity by natural products and derivatives. J. Diabetes Res. 2016: 1–12.

Sciacca, M.F., Chillemi, R., Sciuto, S., Greco, V., Messineo, C., Kotler, S.A., Lee, D.K., Brender, J.R., Ramamoorthy, A., La Rosa, C., et al. (2018). A blend of two resveratrol derivatives abolishes hIAPP amyloid growth and membrane damage. Biochim. Biophys. Acta Biomembr. 1860: 1793–1802.

Semwal, D.K., Semwal, R.B., Combrinck, S., and Viljoen, A. (2016). Myricetin: a dietary molecule with diverse biological activities. Nutrients 8: 90.

Sgarbossa, A. (2012). Natural biomolecules and protein aggregation: emerging strategies against amyloidogenesis. Int. J. Mol. Sci. 13: 17121–17137.

Sim, L., Jayakanthan, K., Mohan, S., Nasi, R., Johnston, B.D., Pinto, B.M., and Rose, D.R. (2010). New glucosidase inhibitors from an ayurvedic herbal treatment for type 2 diabetes: structures and inhibition of human intestinal maltase-glucoamylase with compounds from Salacia reticulata. Biochemistry 49: 443–451.

Singh, U.C. and Kollman, P.A. (1984). An approach to computing electrostatic charges for molecules. J. Comput. Chem. 5: 129–145.

Stanković, I.M., Niu, S., Hall, M.B., and Zarić, S.D. (2020). Role of aromatic amino acids in amyloid self-assembly. Int. J. Biol. Macromol. 156: 949–959.

Stefani, M. and Rigacci, S. (2013). Protein folding and aggregation into amyloid: the interference by natural phenolic compounds. Int. J. Mol. Sci. 14: 12411–12457.

Stridsberg, M. and Wilander, E. (1991). Islet amyloid polypeptide (IAPP) a short review. Acta Oncol. 30: 451–456.

Sun, A.Y., Wang, Q., Simonyi, A., and Sun, G.Y. (2010). Resveratrol as a therapeutic agent for neurodegenerative diseases. Mol. Neurobiol. 41: 375–383.

Tu, L.H. and Raleigh, D.P. (2013). Role of aromatic interactions in amyloid formation by islet amyloid polypeptide. Biochemistry 52: 333–342.

Tu, L.H., Young, L.M., Wong, A.G., Ashcroft, A.E., Radford, S.E., and Raleigh, D.P. (2015). Mutational analysis of the ability of resveratrol to inhibit amyloid formation by islet amyloid polypeptide: critical evaluation of the importance of aromatic–inhibitor and histidine–inhibitor interactions. Biochemistry 54: 666–676.

Van Der Spoel, D., Lindahl, E., Hess, B., Groenhof, G., Mark, A.E., and Berendsen, H.J. (2005). GROMACS: fast, flexible, and free. J. Comput. Chem. 26: 1701–1718.

Velander, P., Wu, L., Ray, W.K., Helm, R.F., and Xu, B. (2016). Amylin amyloid inhibition by flavonoid baicalein: key roles of its vicinal dihydroxyl groups of the catechol moiety. Biochemistry 55: 4255–4258.

Wang, Z.H., Kang, K.A., Zhang, R., Piao, M.J., Jo, S.H., Kim, J.S., Kang, S.S., Lee, J.S., Park, D.H., and Hyun, J.W. (2010). Myricetin suppresses oxidative stress-induced cell damage via both direct and indirect antioxidant action. Environ. Toxicol. Pharmacol. 29: 12–18.

Zelus, C., Fox, A., Calciano, A., Faridian, B.S., Nogaj, L.A., and Moffet, D.A. (2012). Myricetin inhibits islet amyloid polypeptide (IAPP) aggregation and rescues living mammalian cells from IAPP toxicity. Open Biochem. J. 6: 66–70.

Zraika, S., Hull, R.L., Udayasankar, J., Aston-Mourney, K., Subramanian, S.L., Kisilevsky, R., Szarek, W.A., and Kahn, S.E. (2009). Oxidative stress is induced by islet amyloid formation and time-dependently mediates amyloid-induced beta cell apoptosis. Diabetologia 52: 626–635.

Supplementary material: The online version of this article offers supplementary material (https://doi.org/10.1515/hsz-2020-0176).